34th Annual International Conference of the IEEE EMBS
San Diego, California USA, 28 August - 1 September, 2012

Automated extraction of nested sulcus features from human brain MRI data

Forrest Sheng Bao[1], Joachim Giard[2], Jason Tourville[3] and Arno Klein[4]

***Abstract*—Extracting objects related to a fold in the cerebral cortex ("sulcus features") from human brain magnetic resonance imaging data has applications in morphometry, landmark-based registration, and anatomical labeling. In prior work, sulcus features such as surfaces, fundi and pits have been extracted separately. Here we define and extract nested sulcus features in a hierarchical manner from a cortical surface mesh having curvature or depth values. Our experimental results show that the nested features are comparable to features extracted separately using other methods, and that they are consistent across subjects and with manual label boundaries. Our open source feature extraction software will be made freely available as part of the Mindboggle project (http://www.mindboggle.info).**

I. Introduction

The human cerebral cortex is a very complex folded structure. The infolding or concave portions of the cortical surface are called *sulci* that separate intervening ridges called *gyri*. Morphometric differences in these sulci across individuals might help to classify certain neuropsychiatric illnesses, including schizophrenia [1], Alzheimer's disease (AD) and mild cognitive impairment (MCI) [2], depression [3], and bipolar disorder [4]. Sulci and individual *sulcus features* can be derived from magnetic resonance images (MRI), making it possible to do non-invasive morphometry in humans. We use these features as landmarks in landmark-driven registration for voxel-wise comparison across brain images and as topographical boundaries to delimit anatomical regions in atlas-based labeling for region-based comparison across brain images [5]–[7].

The sulcus features we will focus on in this article is the fundus (*pl. fundi*), a curve that traverses the deepest path along the bottom of a sulcus, as well as dips along the fundus that we will call fundus "pits."

Previous studies focus on extracting a single type of sulcus feature, whether it is a fundus [8]–[10], pits [2], [11], [12], watershed segmentations [13], [14], brain hull curves [15], [16], or medial surfaces [17]. Many researchers represent the cortical surface as a mesh, and assign values to the vertexes of the mesh (a "map") that can provide more morphological and anatomical information for better feature extraction than from a 3-D volume. Different maps have been used to extract individual features. For example, Kao et al. [9] extract fundi using geodesic depth, Li et al. [8] extract fundi using curvature, and Im et al. [2] extract pits from a FreeSurfer [18] convexity map (an approximation of depth based on distances that vertexes move when a cortical mesh is inflated). The BrainVISA software [17] extracts the medial surface in a 3-D image volume from within the space of a sulcus fold, and approximates a fundus as the bottom of a medial surface.

In this article, we explore a new way to extract sulcus features. We do not define features independently but instead hierarchically, resulting in a set of nested features: fundus pits lie on fundus curves while fundus curves lie at the bottom of sulcus surfaces. Sulcus surfaces are extracted first, then pits and finally fundi connected by the pits, as shown in Fig. 1.

Compute depth map
⇓
Extract sulci
⇓
Extract fundus pits
⇓
Extract fundi

Fig. 1: Hierarchical pipeline to extract nested features

There are several advantages to representing features as nested hierarchies. A set of related features will be more distinctive than each type of feature alone, raising the possibility of distinguishing individuals or groups based on morphometry, and improving feature matching and landmark-based registration across brains. Nesting features is also a more efficient way of representing properties (curvature, depth, etc.) of each feature. Nesting features will help us in the longer term to test various hypotheses that we otherwise could not test, such as: (1) the position of a feature in its nested hierarchy will help to predict how variable the structure is across individuals, and (2) when differences related to a disorder are detectable between two groups for a given structure, the structure's position in its nested hierarchy can predict how subtle or pathological the condition is.

We present a nested feature extraction pipeline that can extract features using different maps, although we choose to use a "travel depth" map based on an accurate measure of depth [19], [20]. To evaluate our feature extraction pipeline, we visually and numerically compare features that we extract with those extracted by other methods and with manual label boundaries drawn by expert anatomists. In this study, we have found that our nested features are comparable to those

*This project was funded by NIH R01 grant MH084029.

[1]F. S. Bao is with Depts. of Computer Science and Electrical Engineering, Texas Tech University, Lubbock, Texas forrest.bao@gmail.com

[2]J. Giard is with Institute of Information and Communication Technologies, Electronics and Applied Mathematics, Université Catholique de Louvain, Louvain, Belgium joachim.giard@uclouvain.be

[3] J. Tourville is with Dept. of Speech, Language, and Hearing Sciences, and Center for Computational Neuroscience and Neural Technology, Boston University, Boston, Massachusetts jaytour@gmail.com

[4]A. Klein is with New York Psychiatric Institute, Columbia University, New York, New York arno@binarybottle.com

extracted separately by existing approaches, and our results are consistent across subjects and with manual label boundaries. The rest of the paper is organized as follows: Section II provides definitions and algorithms to hierarchically extract nested features, Section III evaluates the resulting features visually and numerically, and Section IV concludes the paper.

II. Methods

Our nested feature extraction pipeline takes as input a mesh of vertexes and edges representing the cortical surface, which may be generated from a T1-weighted MRI by different software packages such as FreeSurfer [18], Caret [21], and BrainVISA [17]. At least one map on the mesh is needed to continue the pipeline. A map may come from a software application other than the one that computes the mesh. Our pipeline can extract different features using different maps, for example sulci with a curvature map and pits with a travel depth map. In this article, we use an external gray matter (triangular) surface mesh from FreeSurfer and compute a travel depth map for each hemisphere in each subject. We also use FreeSurfer to compute curvature and convexity maps in our evaluation to compare our results with other methods that rely on these maps.

A. Travel Depth Map

From a point on a surface, travel depth is defined as the shortest distance from that point to a reference surface along a path that does not run through the interior of the surface [20]. We have recently adapted this measure of depth for use with brain surfaces [19]. We compute the reference surface, which must closely wrap over the cortical surface, by performing a morphological closing operation on the cortical surface with a radius of 5mm. We then normalize depth values so that they lie between 0 and 1 (Fig. 2 and Fig. 3).

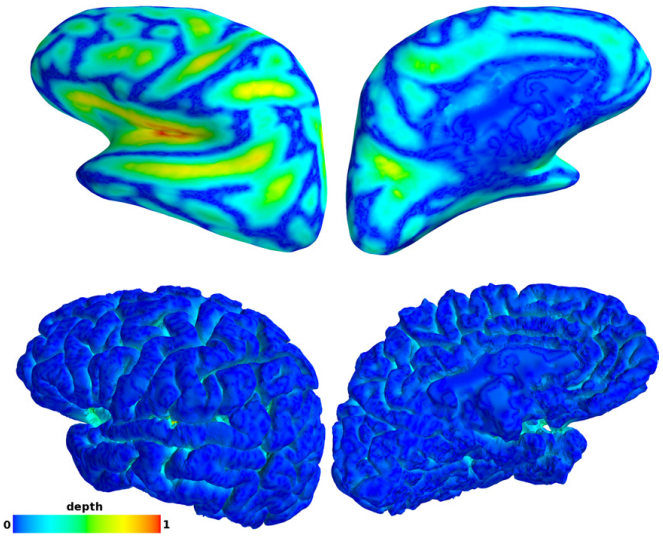

Fig. 2: Normalized travel depth on lateral side (left column) and medial side (right column) of an inflated (top row) and uninflated (bottom row) left cerebrum.

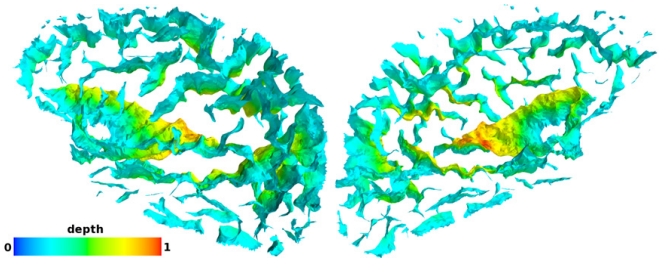

Fig. 3: Sulci on lateral side (left) and medial side (right) of a left cerebrum, colored by normalized travel depth (increasing depth from blue to red).

B. Sulcus Extraction

We separate sulci and gyri by thresholding a given map, in our case the travel depth map. A proper reference surface for computing a travel depth map should provide a natural separation between sulci and gyri: portions of the mesh that are also on the reference surface have zero depth and are gyri, and the remaining portions are sulci. Thus, the threshold is 0. Due to precision errors, in this article we consider any vertex deeper than 0.2 to be a *sulcus vertex*.

C. Pit Extraction

We define pits as sulcus vertexes that are local depth maxima (i.e., no neighbor deeper than itself). Our pit extraction algorithm sorts sulcus vertexes by their depth values to quickly pull out a set of vertexes deeper than any given vertex, then checks whether any neighbor of the given vertex is in the set. If not, the given vertex is considered a pit.

For every sulcus, we run Algorithm 1 to extract pits. At first, vertexes are sorted by their depth values and stored in a stack S with greatest value on top and smallest value at bottom. Two empty arrays/lists are initialized, $Popped$ to store vertexes popped (removed) from S, and $Pits$ to store pits. Then we start popping the stack S. For every vertex v, we add v into $Popped$. If v has no neighbor in $Popped$, we add v into $Pits$. The algorithm stops when stack S is empty.

D. Fundus Extraction from Pits

We define a fundus as a set of mesh edges that connect all pits within one sulcus while maximizing the total depth along its path. In other words, a fundus is a minimum spanning tree (MST) with respect to negative depth (thus maximizing depth) of all fundus pits within the same sulcus. For each sulcus, we have only one fundus. We use Prim's algorithm to construct an MST [22]. Since we want to maximize the depth on the tree, we define the weight of every edge as the negative average of the depth values of its two terminal vertexes.

Because the complexity of constructing an MST is $O(E \lg V)$ where E is the number of edges and V is the number of vertexes, to speed up the computation we first decimate the original mesh by Algorithm 2. For every vertex that is not a pit, we remove it with a probability of 0.8 (Thr

Algorithm 1: Pit extraction in a surface mesh (e.g., within a sulcus)

Input: a graph (V, E) where V are vertexes and E are edges, and depth values of all vertexes in V
Output: vertexes considered as pits

Initialize two empty lists $Popped$ and $Pits$
S := vertexes sorted by depth value
while S *is not empty* **do**
    v := S.pop()
    Add v into Popped
    if v *has no neighbor in* $Popped$ **then**
        Add v into $Pits$
    end
end
return $Pits$

in Algorithm 2) to decrease computation time. To ensure the connectivity of the sulcus, we do not remove a vertex that has a neighbor which has been removed, as illustrated in Fig. 4.

Algorithm 2: Mesh decimation

Input: a graph (V, E) where V are vertexes and E are edges, and a threshold Thr in $[0, 1]$
Output: a graph (V', E')

Initialize an empty list $Removed$
V':= V
E':= E
foreach *vertex* v *in* V **do**
    Rnd:= a randomly generated number in $[0, 1]$
    if v *is a pit* **then** continue
    else if v *has a neighbor in* $Removed$ **then** continue
    else if $Rnd > Thr$ **then** continue
    else
        remove v from V'
        remove all edges in E' connected to v
        Add v into $Removed$
    end
end
return (V', E')

The last step for fundus extraction is MST pruning. The MST constructed above connects all vertexes on a decimated mesh, including non-pit vertexes. The purpose of MST pruning is to remove all subtrees that have no pits. A vertex of degree equal to 1 is a *terminal vertex* and degree greater than 2 is called a *branching vertex*. For every terminal vertex, we remove edges from it until a pit or a branching node is reached. The algorithm ends when all terminal vertexes are pits. Fig. 5 shows an example of how a subtree with two branches are removed.

III. Evaluation

Since our nested feature extraction pipeline works with various maps, including curvature and convexity maps used by other groups, we compared our feature extraction with theirs on the same maps. We used 12 brains of healthy subjects in the CUMC12 dataset (http://www.mindboggle.info/data/) [7]. For our visual comparison, we used a variety of maps to extract features to show the flexibility of our pipeline. Due to page limitations, we are not able to show all results obtained using different maps, but they are similar. We then numerically compare fundi extracted by different approaches.

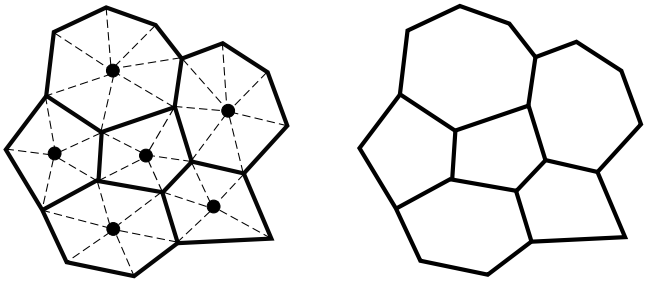

Fig. 4: Mesh decimation. A portion of the original mesh is on the left and the decimated result is on the right. Solid dots are vertexes chosen randomly to be removed. Dashed lines are edges to be removed. To keep connectivity, neighbors of solid dots are kept.

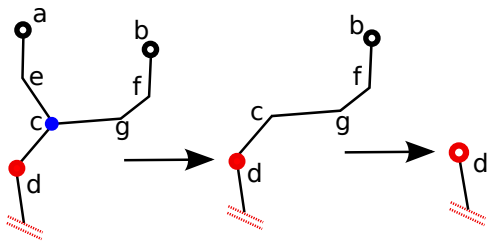

Fig. 5: MST pruning. Black edges represent MST paths (visually truncated at the red dashed lines). The original subtree has two terminal vertexes a and b, branching vertex c and a pit d. a is chosen first and edges $a-e$ and $e-c$ are removed until branching vertex c is reached. After that c is no longer a branching vertex. Then path $b-f-g-c-d$ is removed until pit d is reached. In the end, d becomes a new terminal vertex.

.

The approaches under comparison (Kao et al.'s software was not available):

- BrainVISA [17], to extract *ribbons and fundi* from a *3-D volume*
- Im et al. [2], to extract *sulci and pits* from a *convexity map* on an *external cortical surface*
- Li et al. [8], to extract *fundi* from a *curvature map* on a *gray/white matter surface*
- Our nested approach, to extract *sulci, fundi and pits* from *various maps* on an *external cortical surface*

A. Visual Comparison

Fig. 6 shows the three nested features extracted by our pipeline, namely sulci, fundi and pits, from a mean curvature

map.

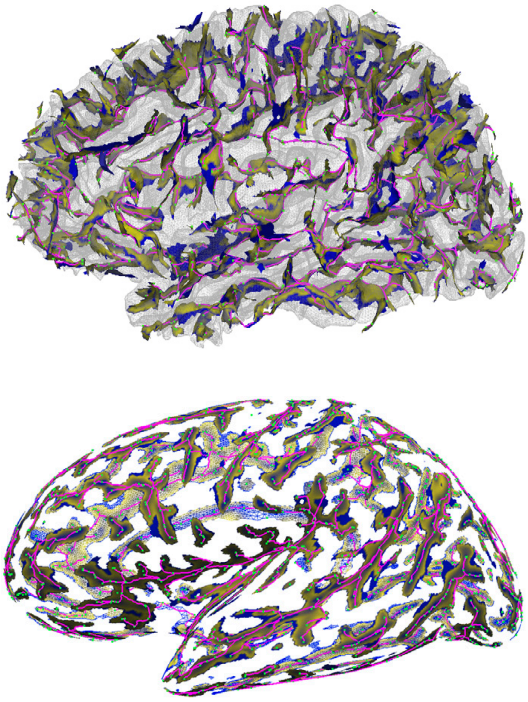

Fig. 6: Sulci (yellow-blue), fundi (magenta), and pits (green) from an uninflated (top) and inflated (bottom) left cortical surface.

Fig. 7 provides a gradient transparent view of sulci and pits as a face validity check to make sure the locations of our pits (and fundi that connect them) are at the bottom of sulci.

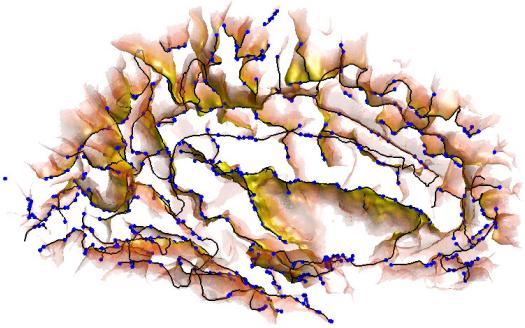

Fig. 7: Sulci, fundi (black curves) and pits (blue dots) from a left cortical surface (medial view). Color indicates convexity, and transparency increases monotonically with convexity to enhance areas of high convexity.

Fig. 8 overlays fundi extracted by three different methods. Our fundi are very similar to Li et al.'s while BrainVISA's fundi overlap in many places with those of the other two methods. We used a curvature map to extract our fundi because it is the same map that Li et al. use.

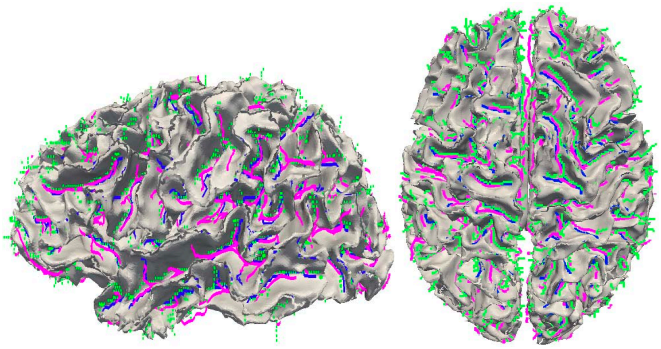

Fig. 8: Our fundi (magenta, from mean curvature), Li et al.'s fundi (blue), and BrainVISA's fundi (green) on a white matter surface in a lateral view of a left hemisphere (left) and top view of the brain (right).

Fig. 9 shows fundi extracted by our pipeline using 3 different maps – travel depth, convexity and curvature. These fundi are shown overlaid atop manual labels. The main branches of the fundi from all three maps are closely aligned with manual label boundaries.

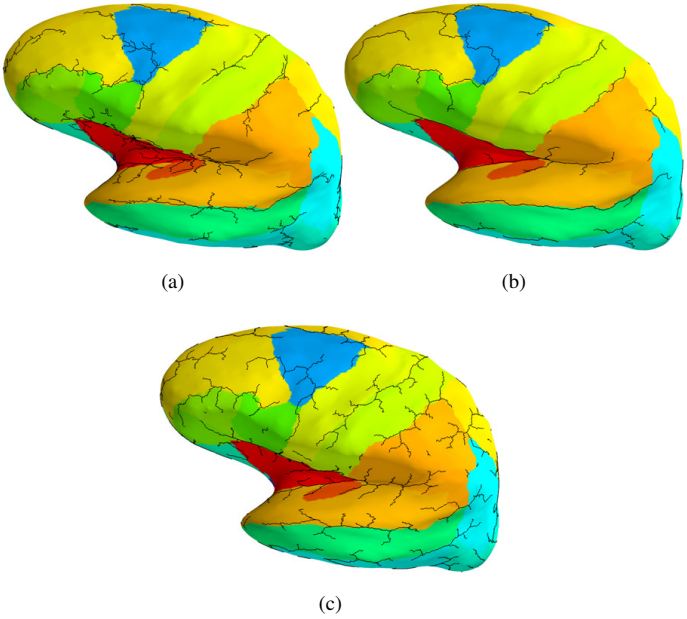

Fig. 9: Manual labels and fundi extracted from (a) travel depth, (b) convexity, and (c) curvature maps on an inflated left hemisphere. (Colors indicate different anatomical regions.)

B. Numerical Comparison

We used the CUMC12's 12 subject images and manual labels for our numerical comparison. In the following two tests, we compare features extracted by different approaches.

Test 1: Is a given type of feature consistent across subjects?

We measured Hausdorff distance between fundus curves in co-registered subjects.

Test 2: Are features consistent with label boundaries? We measured Hausdorff distance between fundus curves and manual label borders.

Only fundus results are reported for both tests, since pits results are biased in favor of the number of pits generated, sulci are defined differently and are computed on different surfaces, and medial surfaces are currently generated only by BrainVISA. The results are very similar across fundus extraction algorithms according to Table I. To minimize the error from using different maps, we used the same curvature map as Li et al. for our method.

TABLE I: Fundus consistency (mean±SD)

	This paper	BrainVISA	Li et al.
Test 1	2.45 ± 1.64 mm	2.16 ± 1.57 mm	2.47 ± 1.66 mm
Test 2	4.34 ± 3.65 mm	4.48 ± 3.28 mm	3.47 ± 2.37 mm

IV. Conclusion

In this paper, we present and evaluate an automated, nested feature extraction pipeline. This pipeline can make use of a variety of measures on a cortical surface mesh, including curvature, convexity, and our own travel depth. Experimental results show that our nested features are comparable to individual features extracted separately by other algorithms as measured by their consistency across subjects, and consistency with manual label boundaries. In future work, we will prune and smooth fundi extracted from our travel depth map, and constrain sulcus medial surface extraction to "grow" from our fundi. The software implementation of our feature extraction algorithms will be released as part of the Mindboggle project at http://www.mindboggle.info

Acknowledgments

This research is funded by NIMH R01 grant MH084029. Forrest's work is also supported by ARMWorks Inc (Seattle, WA). Jocahim is funded by the Walloon Region (Belgium) grant 1017266 ("InVivoIGT"). The authors would like to thank Yrjö Häme and Noah Lee for helping to make Figs. 6-8, and Gang Li and Kiho Im for providing their software for the evaluation. This research used a computing cluster at the High Performance Computing Center of Texas Tech University.

References

[1] A. Cachia, M.-L. Paillère-Martinot, A. Galinowski, D. Januel, R. de Beaurepaire, F. Bellivier, E. Artiges, J. Andoh, D. Bartrès-Faz, E. Duchesnay, D. Rivière, M. Plaze, J.-F. Mangin, and J.-L. Martinot, "Cortical folding abnormalities in schizophrenia patients with resistant auditory hallucinations," *NeuroImage*, vol. 39, no. 3, pp. 927 – 935, 2008.

[2] K. Im, J.-M. Lee, S. W. Seo, H. K. Sun, S. I. Kim, and D. L. Na, "Sulcal morphology changes and their relationship with cortical thickness and gyral white matter volume in mild cognitive impairment and alzheimer's disease," *NeuroImage*, vol. 43, no. 1, pp. 103–13, Oct. 2008.

[3] M. J. Kempton, Z. Salvador, M. R. Munafo, J. R. Geddes, A. Simmons, S. Frangou, and S. C. R. Williams, "Structural neuroimaging studies in major depressive disorder: Meta-analysis and comparison with bipolar disorder," *Archives of General Psychiatry*, vol. 68, no. 7, pp. 675–690, 2011.

[4] J. Penttilä, A. Cachia, J.-L. Martinot, D. Ringuenet, M. Wessa, J. Houenou, A. Galinowski, F. Bellivier, T. Gallarda, E. Duchesnay, E. Artiges, M. Leboyer, J.-P. Olié, J.-F. Mangin, and M.-L. Paillère-Martinot, "Cortical folding difference between patients with early-onset and patients with intermediate-onset bipolar disorder," *Bipolar Disorders*, vol. 11, no. 4, pp. 361–370, 2009.

[5] A. Klein, S. S. Ghosh, B. Avants, B. Yeo, B. Fischl, B. Ardekani, J. C. Gee, J. Mann, and R. V. Parsey, "Evaluation of volume-based and surface-based brain image registration methods," *NeuroImage*, vol. 51, no. 1, pp. 214 – 220, 2010.

[6] A. Klein, B. Mensh, S. Ghosh, J. Tourville, and J. Hirsch, "Mindboggle: Automated brain labeling with multiple atlases," *BMC Medical Imaging*, vol. 5, no. 1, p. 7, 2005.

[7] A. Klein, J. Andersson, B. A. Ardekani, J. Ashburner, B. Avants, M.-C. Chiang, G. E. Christensen, D. L. Collins, J. Gee, P. Hellier, J. H. Song, M. Jenkinson, C. Lepage, D. Rueckert, P. Thompson, T. Vercauteren, R. P. Woods, J. J. Mann, and R. V. Parsey, "Evaluation of 14 nonlinear deformation algorithms applied to human brain mri registration," *NeuroImage*, vol. 46, no. 3, pp. 786 – 802, 2009.

[8] G. Li, L. Guo, J. Nie, and T. Liu, "An automated pipeline for cortical sulcal fundi extraction." *Medical image analysis*, vol. 14, no. 3, pp. 343–59, Jun. 2010.

[9] C.-Y. Kao, M. Hofer, G. Sapiro, J. Stem, K. Rehm, and D. A. Rottenberg, "A geometric method for automatic extraction of sulcal fundi," *IEEE transactions on medical imaging*, vol. 26, no. 4, pp. 530 – 540, Apr. 2006.

[10] G. Le Goualher, E. Procyk, D. L. Collins, R. Venugopal, C. Barillot, and A. C. Evans, "Automated extraction and variability analysis of sulcal neuroanatomy," *IEEE Transactions on Medical Imaging*, vol. 18, no. 3, pp. 206 – 217, march 1999.

[11] G. Lohmann, D. Y. von Cramon, and A. C. F. Colchester, "Deep sulcal landmarks provide an organizing framework for human cortical folding," *Cerebral Cortex*, vol. 18, no. 6, pp. 1415–1420, 2008.

[12] J. RÉGIS, J.-F. MANGIN, T. OCHIAI, V. FROUIN, D. RIVIÉRE, A. CACHIA, M. TAMURA, and Y. SAMSON, "Sulcal root generic model: a hypothesis to overcome the variability of the human cortex folding patterns," *Neurologia medico-chirurgica*, vol. 45, no. 1, pp. 1–17, 2005.

[13] M. Rettmann, X. Han, C. Xu, and J. Prince, "Automated sulcal segmentation using watersheds on the cortical surface," *NeuroImage*, vol. 15, no. 2, pp. 329–344, 2002.

[14] G. Lohmann and D. Y. von Cramon, "Automatic labelling of the human cortical surface using sulcal basins," *Medical Image Analysis*, vol. 4, no. 3, pp. 179 – 188, 2000.

[15] M. L. Jouandet, M. J. Tramo, D. M. Herron, A. Hermann, W. C. Loftus, J. Bazell, and M. S. Gazzaniga, "Brainprints: computer-generated two-dimensional maps of the human cerebral cortex in vivo," *Journal of Cognitive Neuroscience*, vol. 1, no. 1, pp. 88–117, 1989.

[16] G. Lohmann, "Extracting line representations of sulcal and gyral patterns in MR images of the human brain," *IEEE Transactions on Medical Imaging*, vol. 17, no. 6, pp. 1040 –1048, dec. 1998.

[17] J.-F. Mangin, V. Frouin, I. Bloch, J. Régis, and J. López-Krahe, "From 3d magnetic resonance images to structural representations of the cortex topography using topology preserving deformations," *Journal of Mathematical Imaging and Vision*, vol. 5, no. 4, pp. 297–318, Dec. 1995.

[18] A. Dale, B. Fischl, and M. Sereno, "Cortical surface-based analysis i: Segmentation and surface reconstruction," *NeuroImage*, vol. 9, no. 2, pp. 179–194, 1999.

[19] J. Giard, F. S. Bao, and A. Klein, "Travel depth: a new measure of depth for brain surfaces," Mar. 2012, manuscript under reviewing.

[20] J. Giard, P. Rondao Alface, J. Gala, and B. Macq, "Fast surface-based travel depth estimation algorithm for macromolecule surface shape description," *Computational Biology and Bioinformatics, IEEE/ACM Transactions on*, vol. 8, no. 1, pp. 59–68, 2011.

[21] D. C. van Essen, "Cortical cartography and Caret software," *NeuroImage*, 2011, in printing.

[22] T. H. Cormen, C. E. Leisserson, R. L. Rivest, and C. Stein, *Introduction to Algorithms*, 2nd ed. MIT Press, 2001.